Biophysical *Journal*
Article

Biophysical Society

Electrostatic interaction optimization improves catalytic rates and thermotolerance on xylanases

Vinícius de Godoi Contessoto,[1,2,3] Felipe Cardoso Ramos,[1] Ricardo Rodrigues de Melo,[1] Vinícius Martins de Oliveira,[4] Josiane Aniele Scarpassa,[1] Amanda Silva de Sousa,[1] Letıcia Maria Zanphorlin,[1] Gabriel Gouvea Slade,[5] Vitor Barbanti Pereira Leite,[3,*] and Roberto Ruller[6]

[1]Brazilian Biorenewables National Laboratory, Brazilian Center for Research in Energy and Materials, Campinas, São Paulo, Brazil; [2]Center for Theoretical Biological Physics, Rice University, Houston, Texas; [3]Department of Physics, Institute of Biosciences, Letters and Exact Sciences, São Paulo State University, São José do Rio Preto, São Paulo, Brazil; [4]Brazilian Biosciences National Laboratory, Brazilian Center for Research in Energy and Materials, Campinas, São Paulo, Brazil; [5]Theoretical Biophysics Laboratory, Institute of Exact Sciences, Natural and Education, Federal University of Triângulo Mineiro, Uberaba, Minas Gerais, Brazil; and [6]Microorganisms and General Biochemistry Laboratory, Institute of Bioscience, Federal University of Mato Grosso do Sul, Campo Grande, Mato Grosso do Sul, Brazil

ABSTRACT Understanding the aspects that contribute to improving proteins' biochemical properties is of high relevance for protein engineering. Properties such as the catalytic rate, thermal stability, and thermal resistance are crucial for applying enzymes in the industry. Different interactions can influence those biochemical properties of an enzyme. Among them, the surface charge-charge interactions have been a target of particular attention. In this study, we employ the Tanford-Kirkwood solvent accessibility model using the Monte Carlo algorithm (TKSA-MC) to predict possible interactions that could improve stability and catalytic rate of a WT xylanase ($XynA^{WT}$) and its M6 xylanase ($XynA^{M6}$) mutant. The modeling prediction indicates that mutating from a lysine in position 99 to a glutamic acid (K99E) favors the native state stabilization in both xylanases. Our lab results showed that mutated xylanases had their thermotolerance and catalytic rate increased, which conferred higher processivity of delignified sugarcane bagasse. The TKSA-MC approach employed here is presented as an efficient computational-based design strategy that can be applied to improve the thermal resistance of enzymes with industrial and biotechnological applications.

SIGNIFICANCE To perform protein engineering and design optimized enzymes is a challenging task. Understanding the balance of several interactions acting within the enzyme can help select good mutants. Based on a first-principles electrostatic optimization approach, the Tanford-Kirkwood solvent accessibility model using the Monte Carlo algorithm (TKSA-MC) method suggests residues substitutions to reform the enzyme interactions in its native conformation. Mutation candidates indicated by the TKSA-MC web server were investigated in a wet lab. The results corroborate with the predictions and indicate that TKSA-MC can be a powerful tool for designing more thermal stable and active enzymes.

INTRODUCTION

The biochemical properties of proteins depend on the balance of several interactions. The knowledge of principles that govern these interactions is fundamental to designing optimized proteins for industrial and biotechnological purposes (1–4). Among these interactions, the charge-charge interplay within a protein is crucial for stabilizing the native state (5–10). Solution conditions, such as salt concentration and pH, also tend to influence protein stability significantly. The optimum balance between electrostatic effects can lead the protein to a more thermal stable state (11–15).

Over the years, the quest for novel enzymes with biotechnological application potential has involved various complementary approaches. These strategies include mining enzyme variants from microorganisms living in extreme conditions (extremophiles) (16) and mimicking evolution in the laboratory by employing directed enzyme evolution (17,18) to develop more stable and resistant enzyme variants for industrial purposes (19–21). Recently, the application of bioinformatics tools and physical modeling has been incorporated as a rational strategy for predicting optimizing mutations (4,22,23). To predict the free-energy change upon mutations using computational approaches is a nontrivial

Submitted October 1, 2020, and accepted for publication March 23, 2021.

*Correspondence: vitor.leite@unesp.br

Vinícius de Godoi Contessoto and Felipe Cardoso Ramos contributed equally to this work.

Editor: Margaret Cheung.

https://doi.org/10.1016/j.bpj.2021.03.036

challenge (4). Optimization of the protein charge-charge interactions has shown to be an effective method for thermal stability improvement (24). Makhatadze and co-workers investigated the optimization of electrostatic interactions via directed mutations presenting an increase of thermal stability for different proteins (25,26). The methodology calculates the electrostatic energy contribution for each ionizable residue using the Tanford-Kirkwood solvent accessibility model (TKSA) (27–30). The method indicates a few residues to be mutated to increase the thermal stability of proteins. The criteria follow residues contributing to positive energy (destabilizing interactions) with exposed to solvent (solvent-accessible surface area greater than 50%). The choice for mutating a residue exposed to the solvent is to avoid modifying the protein three-dimensional (3D) structure drastically. Recently, our group implemented this methodology as a webtool using the Metropolis Monte Carlo algorithm (TKSA-MC) (31). This approach speeds up the sampling of the different protonation states of each ionizable residue in the investigated protein. The TKSA-MC allows us now to explore more complex systems. One of the advantages of optimizing the protein charge-charge interactions is suggesting mutations based on pH and salt concentration conditions that the system requires. Even though many successful cases employing this methodology were reported, there is a lack of studies regarding this application in a more complex system such as bigger enzymes or protein complexes.

For instance, an interesting and crucial system is the xylanase belonging to glycoside hydrolase family 11 (GH11). GH11 enzymes are a notoriously abundant family in plant cell-wall-degrading microorganisms. These enzymes are mainly involved in xylan degradation, which is the major hemicellulosic polysaccharide (32). The usage of GH11 enzymes is essential in different biotechnological areas, especially for the successful implementation of sugar-based biorefinery processes. In previous studies (17,18), directed evolution techniques were used to improve the thermal stability of the xylanase GH11 from *Bacillus subtilis* (XynA). Two generations of random mutant libraries generated by error-prone PCR coupled with a single generation of DNA shuffling produced a series of mutant proteins with increasing thermostability. All mutations were located at the surface of these enzymes, suggesting that the decrease in the ΔC_p includes effects arising from the protein-solvent interface.

Herein, the TKSA-MC approach was employed to select mutations for optimizing the electrostatic interactions on the surface of WT xylanase ($XynA^{WT}$) and its M6 xylanase ($XynA^{M6}$) variant ($XynA^{WT}$ with six mutations—Q7H, S22P, T44A, I51V, I107L, and S179C—generated by directed enzyme evolution (17,18)). From an enzyme engineering perspective, electrostatic interactions affect enzyme activity in different ways, such as its thermal stability T_m, catalytic rate, thermotolerance, and processivity of delignified sugarcane. However, the direct correspondence between electrostatic contributions and these enzyme parameters is unclear. Nevertheless, electrostatic interaction optimization of the native state is expected to improve enzyme functional parameters, and it can be a valuable approach in enzyme improvement.

The TKSA-MC simulations predicted the mutation of lysine in position 99 (K99) as a potential candidate to be mutated and optimize both xylanases. As a validation, we performed different wet-lab experiments, including thermal stability studies, lignocellulosic biomass saccharification, and functional assays. To the best of our knowledge, these are the biggest proteins investigated so far using the TKSA-MC approach.

MATERIALS AND METHODS

Proteins

The structural coordinates of $XynA^{WT}$ (PDB: 1XXN) were extracted from the Protein Data Bank (PDB; https://www.rcsb.org). $XynA^{WT}$ is composed of 185 amino acid residues, with 23 of them ionizable, having its 3D structure organized as an α-helix and two twisted β-sheets forming a jellyroll fold (Fig. 1). The M6 xylanase ($XynA^{M6}$) has six mutations—Q7H, S22P, T44A, I51V, I107L, and S179C (17,18,35)—and had its tridimensional model built using Modeler software (36).

Computational analysis

Tanford-Kirkwood (TK) is a continuum electrostatic model that considers the protein as a sphere with low dielectric constant (ε_p) and radius b (28). A solvent accessibility correction of each ionizable residue was introduced in the TK model by Shire and co-workers to adjust cavities and the interface between the solvent and the protein (29). Including this correction, the method is named the TKSA model (29,37,38). The electrostatic interaction energy U between charged groups i and j is given by

$$U_{ij} = e^2\left(\frac{A_{ij} - B_{ij}}{2b}\frac{C_{ij}}{2a}\right)\left(1 - SA_{ij}\right), \tag{1}$$

where e is the elementary charge; a is the radius of ionic exclusion; and A_{ij}, B_{ij}, and C_{ij} are parameters calculated via the analytical solution of the TK model, which are functions of the distance between the residues i and j, the dielectric constants, and the salt concentration. SA_{ij} is the average of the surface accessibility of the pair of residues (29,30,38). After the calculation of the electrostatic energy between all ionizable residue pairs (39,40), the free energy ΔG_N of all possible protonation states of the protein in its native state is calculated by

$$\Delta G_N(\chi) = RT(\ln 10)\sum_{i=1}^{n}(q_i + x_i)\mathrm{p}K_{\mathrm{a,ref,i}} + \frac{1}{2}\sum_{i,j=1}^{n} U_{ij}(q_i + x_i)\left(q_j + x_j\right), \tag{2}$$

where R is the ideal gas constant, T is the temperature, i and j are the indexes of the ionizable residues, n is the number of ionizable residues, q is the charge of the residue in its deprotonated state, x is 0 or 1 depending on the protonation state, and $\mathrm{pK_{a,\ ref}}$ is the reference pK_a-value. The $pK_{a,\ ref}$-values are 3.6 for the C-terminus, 4.0 for aspartic acid, 4.5 for glutamic

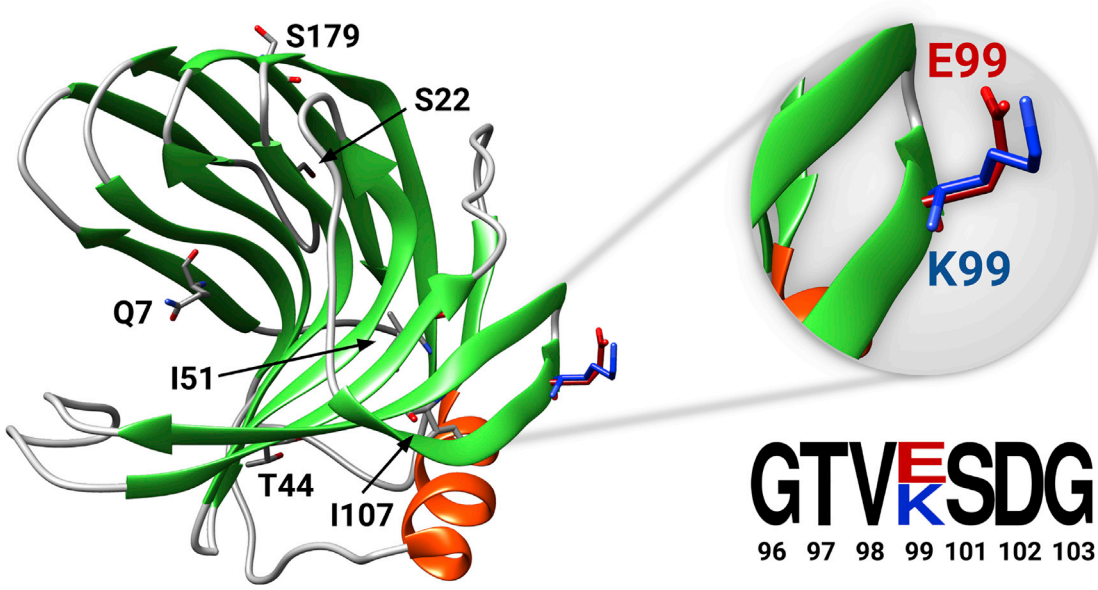

FIGURE 1 The 3D structure of the WT xylanase ($XynA^{WT}$; PDB: 1XXN) built using Chimera software (33). Highlighted is the mutation K99E investigated in this work, indicating how exposed the residue side chain is to the solvent. The M6 variant residues (Q7, S22, T44, I51, I107, and S179) are also presented in the structure. The letters indicate the region where the mutation occurred (34). To see this figure in color, go online.

acid, 6.3 for histidine, 7.5 for the N-terminus, 10.6 for lysine, and 12.0 for arginine. The probability of the protein assumes a particular protonation state is given by

$$\rho_N(\chi) = \frac{1}{Z_N}\exp\left[-\frac{\Delta G_N(\chi)}{RT} - \nu(\chi)(\ln 10)\mathrm{pH}\right], \quad (3)$$

where Z_N is the partition function of the protein in its native state and ν is the number of ionizable residues in the protonation state χ. The mean of the electrostatic energy W_{qq} is calculated over all protonation state and weighted by $\rho_N(\chi)$:

$$\langle W_{qq}\rangle = \sum_{\chi}\left[\frac{1}{2}\sum_{i,j=1}^{n} U_{ij}(q_i + x_i)(q_j + x_j)\right]\rho_N(\chi) \quad (4)$$

The contribution of the electrostatic free energy ΔG_{qq} can be calculated approximately by the negative of Eq. 4, i.e., $\Delta G_{qq} \approx -\langle W_{qq}\rangle$ (40). The electrostatic free energy ΔG_{qq} was performed using the TKSA-MC web server (http://tksamc.df.ibilce.unesp.br; (31)). It must be stressed that the TKSA-MC addresses only the electrostatic contributions to the free energy, which means entropic contributions are not considered. Currently, there is no reliable method to estimate entropic changes upon mutations or, equivalently, to evaluate the changes in specific heat, which would be required to predict Gibbs free-energy changes fully (25,41). However, because charge-charge and charge-solvent interactions play a fundamental role in thermodynamic stability, the TKSA-MC method serves as a guiding tool to probe potential mutations in protein engineering.

Heterologous expression

The genes encoding $XynA^{WT}$, $XynA^{M6}$, and their mutants were codon optimized for expression in *Escherichia coli* cells and synthesized (GenScript, Piscataway, NJ). The sequences were further subcloned into the pET-28a(+) vector (Novagen, Gibbstown, NJ) with an N-terminal His-tag. The constructed vectors were then inserted into *E. coli* BL21 (DE3)-competent cells (Novagen) by heat shock for protein production. The transformed cells were cultured in Luria-Bertani medium (m v^{-1}: 1.0% tryptone, 0.5% yeast extract, and 1.0% NaCl) containing 30 μg mL^{-1} kanamycin. The cultures were grown at 37°C, 250 rpm until the optical density at 600 nm reached a value of 0.6–0.8. The protein expression was induced by 0.5 mM isopropyl β-D-1-thiogalactopyranoside and cultivated for 4 h at 37°C. The cells were harvested by centrifugation at 7500 × *g* (4°C) using a JLA-9.1000 rotor in an Avanti J-25 centrifuge (Beckman Coulter, Brea, CA). Pellets were resuspended in a minimal volume of ice-cold buffer A (20 mM imidazole, 300 mM NaCl, 25 mM sodium phosphate buffer (pH 7.4)) and stored at −20°C.

Purification using affinity chromatography

For enzyme purification, each pellet was treated with lysozyme (0.5 mg mL^{-1}) and phenylmethanesulfonyl fluoride protease inhibitor (1 mM) at room temperature for 20 min, followed by 18 cycles of sonication on ice (10 s pulse on/10 s pulse off) using 30% of the total device (Vibra-Cell; Sonics, Newton, CT) capacity. The cell lysate obtained was centrifuged at 13,000 × *g* for 30 min at 4°C. The supernatant was filtered through a 0.45 μm membrane and injected onto a 5 mL HisTrap HP column (GE Healthcare, Waukesha, WI) previously equilibrated with buffer A coupled to an ÄKTA purifier system (GE Healthcare). Elution of recombinant enzymes was performed by slowly increasing the concentration (v v^{-1}) of buffer B (500 mM imidazole, 300 mM NaCl, 25 mM sodium phosphate buffer (pH 7.4)) on mobile phase. Affinity chromatography samples considered pure by 12% SDS-PAGE verification were pooled and concentrated by ultrafiltration on Amicon Ultra Centrifugal Filter (Millipore, Burlington, MA) with 10 kDa pores. The concentration of the purified enzymes was estimated by ultraviolet absorbance at 280 nm using a Nanodrop device (Thermo Fisher Scientific, Waltham, MA).

Biochemical parameters of recombinant xylanases

The optimum pH was evaluated using xylan from Beechwood (Sigma-Aldrich, St. Louis, MO) in a pH range 3.5–9.5 at 50°C, using the following

buffers: citric acid-sodium citrate (pH 3.5–6.5), monobasic phosphate-dibasic phosphate (pH 7.0–8.0), tris-HCl (pH 8.5), and glycine-NaOH (pH 9.5), at a final concentration of 0.1 M. The optimum temperature was determined in a range of 20–80°C using the best pH of each enzyme. All tests were carried out in 100 μL of reactions containing 50 μL of the substrate (1.0% v v^{-1}), 45 μL of buffer, and 5 μL of pure enzyme. The samples were incubated for 10 min, and then 100 μL of 3,5-dinitrosalicylic acid was added and heated at 95°C for 5 min. The activity was monitored at 540 nm using an Infinite 200 PRO microplate reader (TECAN Group, Männedorf, Switzerland). The highest activity obtained during each experiment was defined as 100% activity. The kinetic parameters were obtained under standard conditions with a series of xylan concentrations (0.16–25 mg mL^{-1}). The final enzyme concentration employed was 0.019 mM $XynA^{WT}$ and $XynA^{K99E}$ or 0.037 mM $XynA^{M6}$ and $XynA^{M6+K99E}$. Kinetic parameters were obtained by sigmoidal fitting using Hill function (Origin 8.1 software). All enzyme assays were performed in triplicate (n = 3).

Biophysical parameters of recombinant xylanases

Circular dichroism (CD) spectra were acquired on a JASCO J-815 spectrometer (Jasco, Tokyo, Japan) controlled by a CDF-426S/15 Peltier temperature control system using a quartz cuvette with a 1 cm pathlength. The enzymes were prepared in 0.1 M sodium citrate buffer (pH 5.0) at a final concentration of 0.3 mg mL^{-1}. All spectra were obtained at 20°C in the range 195–260 nm, with a bandwidth of 2 nm and a response time of 4 s nm^{-1}. CD spectra were buffer subtracted and normalized to mean residue ellipticity. Thermal unfolding experiments were monitored at 218 nm in the temperature range 20–90°C with a scan rate of 1°C min^{-1}. The melting temperatures were determined by sigmoidal fitting using the Boltzmann function (Origin 8.1 software).

Thermotolerance and processivity assay of lignocellulosic biomass

The thermotolerance was determined by measuring the half-life ($t_{1/2}$) of each enzyme, which is defined as the time that the enzyme activity declines to half of the full activity at a specific temperature. The value of the half-life ($t_{1/2}$) was estimated by adjusting the activity data to an exponential decay model. The thermotolerance was evaluated at a temperature 50°C at pH 5.0. The processivity assays of lignocellulosic biomass was explored using the delignified sugarcane bagasse (DSB). The sugarcane bagasse was prepared by alkaline pretreatment (130°C, 30 min, 1.5% m v^{-1} NaOH), yielding a material composed of 60.5 ± 1.1% cellulose, 24.1 ± 0.5% hemicellulose, 9.4 ± 0.1% lignin, and 6.3 ± 2.8% ash. Enzymatic hydrolysis reactions were performed in samples of 1.0 mL containing 5.0% dry biomass (50 mg) and 0.2 filter paper units (FPU) g^{-1} of the enzyme cocktail, supplemented or not with 200 μg $XynA^{WT}$, $XynA^{M6}$, or their mutants. The reactions were done incubated in a hybridization oven at 50°C at pH 5.0 with agitation for 24 h. The fungal enzyme cocktail used in the tests was Celluclast (Novozymes, Krogshoejvej, Denmark). The protein concentration of the fungal cocktail was estimated by the Lowry method (42) using the DC protein kit (BioRad, Hercules, CA). The detection of total reducing sugars was carried out using the 3,5-dinitrosalicylic acid method (43).

RESULTS AND DISCUSSION

TKSA-MC as a prediction tool to increase enzyme native state stability

The TKSA-MC tool was used to predict mutations that could increase the thermal stability of $XynA^{WT}$ and its $XynA^{M6}$ variant. The quantitative analysis of electrostatic interactions in the native state of these proteins was performed at pH 5.0. Fig. 2 displays the electrostatic calculations of WT xylanase and its mutant K99E ($XynA^{K99E}$). Each vertical bar corresponds to the electrostatic free-energy (ΔG_{qq}) contribution of each ionizable residue (x axis) to enzyme stability.

$XynA^{WT}$ has 16 amino acids with a negative value of ΔG_{qq}, which contribute favorably to the stabilization of its native state (Fig. 2 *A*). Among these 16, there are 14 residues plus the charges of the N- and C-termini of the WT enzyme. Moreover, three residues showed energy values close to zero ($\Delta G_{qq} \approx 0.0$), and six residues had a positive value of ΔG_{qq}, contributing unfavorably to its stability. The total electrostatic free energy ΔG_{elec} for the WT enzyme is −83.60 kJ

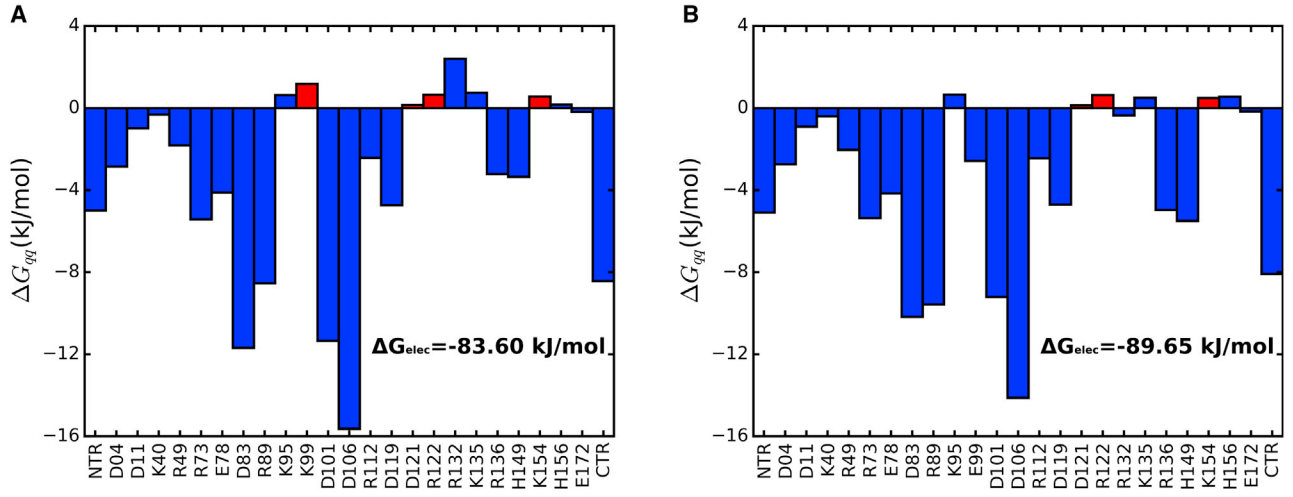

FIGURE 2 Charge-charge interaction energy ΔG_{qq}, in kJ • mol^{-1}, calculated by the TKSA-MC model for each ionizable residue of $XynA^{WT}$ in pH 5.0. The results are shown for $XynA^{WT}$ (*A*) and $XynA^{K99E}$ (*B*). The red bars indicate the residues with the side chain exposed to solvent with SASA ≥ 50% and positive energy contribution to native state stability. To see this figure in color, go online.

• mol^{-1}, and it was calculated as the sum of ΔG_{qq} of all ionizable groups (44–46).

The residues with positive electrostatic free-energy values are associated with the destabilization of the protein native state. Thus, the amino acids K95, K99, R122, R132, K135, and K154 identified with a positive value of ΔG_{qq} were selected. Besides, another criterion used to select the amino acid to be mutated was that it must have a side chain exposed more than 50% to solvent ($\geq$50%). Table 1 shows that residues K99, R122, and K154 have solvent-accessible surface area (SASA) > 50%.

According to Table 1, the residues that follow the criteria to be mutated are K99, R122, and K154. All three have a positive free-energy contribution and have their side chain exposed to solvent more than 50%. These three residues are also highlighted in the red bars in the graph of Fig. 2 *A*. In this work, the residue K99 was chosen to be investigated because of its more negative ΔG_{qq} and higher SASA. Residues R122 and K154 are also possible candidates to be mutated to increase the enzyme thermostability, but they are not explored in this work.

The mutation in the position K99 was performed in silico, removing the positive charge of the lysine side chain and inserting a glutamic acid, which is a negatively charged residue. The choice of the mutation K99E was made to perform a charge inversion in position 99, removing a positive charge and inserting a negative one. The simulation of the mutation K99E in the WT xylanase enzyme was performed, and the electrostatic free-energy graph bar is shown in Fig. 2 *B*. The ΔG_{qq} of position 99 changes from 1.174 kJ • mol^{-1} in the WT enzyme with the lysine to −2.584 kJ • mol^{-1} with the glutamic acid. The total electrostatic free energy ΔG_{elec} changes from −83.60 to −89.65 kJ • mol^{-1} with the mutation K99E, which corresponds to an increase of the electrostatic free-energy stability in ∼7.25%. The effect of the mutation K99E in ΔG_{elec} was not just related to the free-energy stability in position 99 but also connected to the cooperative effect of this charge modification in other enzyme residues, i.e., the mutation K99E contributes to stabilizing the free-energy contribution of different residues. The most significant energy variation due to the cooperative effect mutation K99E occurs in position R132. The ΔG_{qq} changes from 2.395 kJ • mol^{-1} in the WT enzyme to −0.356 kJ • mol^{-1} with the mutation K99E.

TABLE 1 Details of the electrostatic free energy ΔG_{qq} and the SASA are presented for each residue with positive ΔG_{qq} for the enzyme XynA^{WT}

Residue	ΔG_{qq} (kJ • mol^{-1})	SASA (%)
K95	0.633	40.11
K99[a]	1.174[a]	74.75[a]
R122[a]	0.651[a]	73.43[a]
R132	2.395	9.81
K135	0.748	46.54
K154[a]	0.572[a]	72.22[a]

[a]The residues that follow the criteria to be mutated (K99, R122, and K154).

The second system evaluated was the M6 xylanase. The theoretical approach to investigate the XynA^{M6} was similar to that described for the WT enzyme. First, the electrostatic free-energy profile was built, and then the candidate positions with side chain exposed to solvent and positive energy contribution were selected. Fig. 3 *A* presents the bar graph with the electrostatic free-energy profile.

XynA^{M6} has 17 ionizable groups with a negative value of ΔG_{qq}, including the charges of the N- and C-termini, which contribute favorably to protein stability. Besides, two residues showed energy values close to 0 ($\Delta G_{qq} \approx 0.0$), and seven residues were identified with $\Delta G_{qq} > 0.0$. The total electrostatic free energy for the M6 enzyme was −88.09 kJ • mol^{-1}. Similar to XynA^{WT}, the amino acids with a positive value of ΔG_{qq} (K95, K99, R122, R132, K135, K154, and H156) were selected. The values of ΔG_{qq} and the SASA of these residues are described in Table 2.

For the M6 enzyme, three candidates were identified as possible mutation sites: K99, R122, and K154. All of them showed a positive electrostatic free-energy contribution and are exposed to the solvent more than 50% (Table 2). Similar to XynA^{WT}, the position K99 was chosen to carry out the mutations both in simulations and in experiments. The mutation in position K99 was performed in silico, removing the positive charge of the lysine side chain and inserting a negative charge with the glutamic acid. The electrostatic interactions of the K99E mutation in the M6 enzyme were calculated, and Fig. 3 *B* shows its ΔG_{qq} graph bar. The position 99 changes from 1.062 kJ • mol^{-1} in the M6 enzyme with the lysine to −2.437 kJ • mol^{-1} with the glutamic acid. The total electrostatic free energy ΔG_{elec} changes from −88.09 to −93.06 kJ • mol^{-1} with the mutation K99E, which corresponds to an increase of the electrostatic free-energy stability of ∼5.64%. The similar effect of cooperativity with K99E in the WT enzyme was observed in the M6 enzyme. The mutation K99E contributes to stabilizing the free-energy contribution of different residues, and the most significant energy variation also occurs in the position R132. The energy changes from 2.130 kJ • mol^{-1} in the enzyme M6 to −0.497 kJ • mol^{-1} with the mutation K99E.

The mutation K99E promotes improvements in the catalytic rates

XynA^{WT}, XynA^{M6}, and their mutants were expressed in *E. coli* BL21 (DE3) and purified to homogeneity by Ni^{2+}-affinity chromatography. SDS-PAGE analysis indicated that all xylanases migrated as a single dominant band with expected molecular weights (data not shown). Both WT xylanases and mutants were purified in a folded form, as indicated by experiments monitored using CD spectroscopy

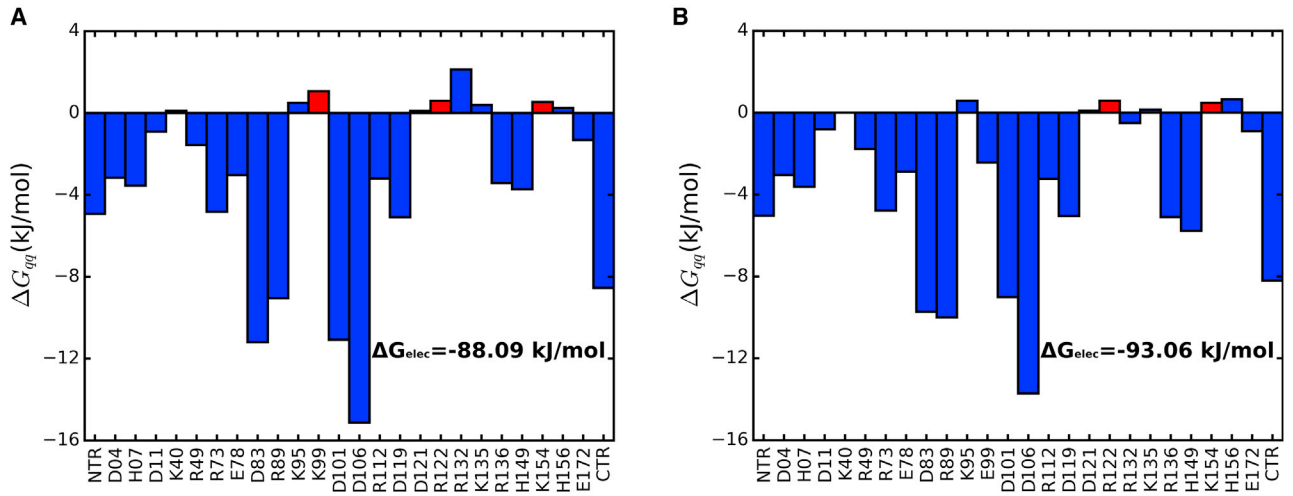

FIGURE 3 Charge-charge interaction energy ΔG_{qq}, in kJ • mol^{-1}, calculated by the TKSA-MC model for each ionizable residue of XynA^{M6} in pH 5.0. The results are presented for the XynA^{M6} (*A*) and M6 enzyme with the mutation K99E XynA$^{M6\ +\ K99E}$. The red bars indicate the residues with the side chain exposed to solvent with SASA $\geq$ 50% and positive energy contribution to native state stability. To see this figure in color, go online.

(Fig. S1). CD analysis also showed that xylanases have a typical β-sheet profile, with minimal molar ellipticity at 218 nm (Fig. S1), as previously reported (47). To better understand the catalytic properties of XynA^{K99E} and XynA$^{M6\ +\ K99E}$ mutants, we characterized the influence of pH and temperature on enzyme activities and investigated their kinetics parameters. As shown in Fig. 4 *A*, the maximal activity plateau of the XynA^{K99E} mutant (pH 6.0) was not altered compared to XynA^{WT}; however, its adaptability to acidic pH regions was slightly expanded. For the XynA$^{M6\ +\ K99E}$ mutant, the pH-dependent profile (pH 6.0) was similar to its nonmutant counterpart. According to the results of ideal temperature assays (Fig. 4 *B*), we found that for all enzymes, including WT xylanases and mutants, the optimum temperature showed no expressive differences. XynA^{WT} and its mutant had optimum activity at 50°C, whereas xylanase M6 (XynA^{M6}) and its mutant were most active at 60°C (Fig. 4 *B*). On the other hand, CD analysis showed that the mutation K99E was able to induce an increase of up to 1°C in the Tm-value in both XynA^{WT} and XynA^{M6} (Fig. 4 *C*). An increase of Tm around 1°C is not a significant increase in the thermostability. The theoretical methodology employed here cannot predict how much the melting temperature variation (ΔTm) due to the mutations will be. The TKSA-MC mutation predictions lead the optimized protein to a more stable native state, but other factors need to be considered for increasing the protein melting temperature. One of those factors is the protein ΔC_p, which is not trivial to predict how it changes upon mutations. TKSA-MC suggests mutation on the protein surface to minimize ΔC_p changes in the protein variant (46) The kinetics parameters of XynA^{K99E} and XynA$^{M6\ +\ K99E}$ mutants were determined using xylan concentrations up to 25 mg • mL^{-1} (Fig. 4 *D*; Table 3). The catalytic rate (k_{cat}) of XynA^{K99E} (528.73 s^{-1}) was 1.08-fold higher than XynA^{WT} (485.11 s^{-1}); however, the half-saturation constant (k_m) of XynA^{K99E} (3.82 ± 0.14 mg • mL^{-1}) was relatively similar in both xylanases (XynA^{WT}; $k_m = 3.34 \pm 0.25$ mg • mL^{-1}). The XynA$^{M6\ +\ K99E}$ also increased its k_{cat} (1.27-fold) compared to the WT counterpart (XynA^{M6}), as well as its k_m-value (1.45-fold; Fig. 4 *D*; Table 3). It was apparent that the mutation K99E contributes to a moderate increase in catalytic rates (k_{cat}) of mutated xylanases. As illustrated, in this study, the mutation K99E not only contributes to slightly increasing the thermal stability of XynA^{WT} and XynA^{M6} xylanases but also to improving the catalytic rates (k_{cat}).

TABLE 2 Details of the electrostatic free energy ΔG_{qq} and the SASA are presented for each residue with positive ΔG_{qq} for the M6 enzyme

Residue	ΔG_{qq} (kJ • mol^{-1})	SASA (%)
K95	0.491	41.31
K99[a]	1.062[a]	73.74[a]
R122[a]	0.588[a]	71.40[a]
R132	2.130	11.30
K135	0.3912	48.45
K154[a]	0.5386[a]	73.78[a]
H156	0.2526	31.64

[a]The residues that follow the criteria to be mutated (K99, R122, and K154).

XynA^{K99E} and XynA$^{M6\ +\ K99E}$ mutants showed better thermotolerance and processivity on pretreated lignocellulosic biomass

The prominent activity of XynA^{WT} and XynA^{M6} xylanases (17,18) under similar conditions to those used for enzymatic hydrolysis in biorefineries led us to explore the industrial potential of their mutants as a complement in fungal enzyme cocktails. Initially, we access the thermal stability of these

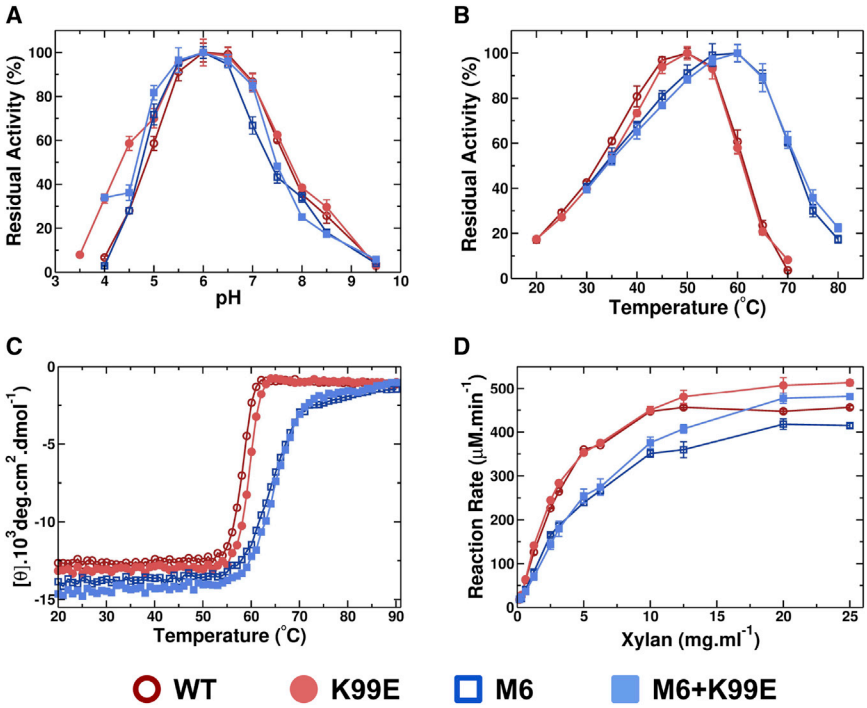

FIGURE 4 Experimental results presenting effects of (*A*) pH and (*B*) temperature on the activity of XynA^{WT}, XynA^{M6}, and mutants. The pH influence was carried out at 50°C using variable buffers (pH 3.5–9.5), and the temperature effect was evaluated from 20 to 80°C. Relative activity (%) was calculated considering the maximal catalytic activity observed for the biological unit of the enzyme. (*C*) Kinetic parameters of XynA^{WT}, XynA^{M6}, and mutants were determined using xylan as substrate under the ideal conditions of each enzyme: pH 6.0 and 50°C for XynA^{WT} and XynA^{K99E} and pH 6.0 and 60°C for XynA^{M6} and XynA$^{M6\ +\ K99E}$. The kinetics parameters were calculated by adjusting the experimental data to the hyperbolic Michaelis-Menten equation. (*D*) Thermal denaturation profiles of XynA^{WT}, XynA^{M6}, and mutants. The profiles were carried out with sodium citrate buffer (20 mM and pH 5.0) and at standardized protein concentrations to 0.3 mg • mL^{-1}. XynA^{WT}, open red circles; e XynA^{K99E}, solid red circles; XynA^{M6}, open blue squares; XynA$^{M6\ +\ K99E}$, solid blue squares. To see this figure in color, go online.

mutants under conditions that simulate saccharification in biorefineries (pH 5.0 and 50°C; Fig. 5 *A*). The results showed that, at 50°C, the mutated xylanases had improved thermal stability compared to their nonmutated proteins (Fig. 5 *A*). The half-life ($t_{1/2}$) of mutant XynA^{K99E} was increased up to threefold higher than XynA^{WT}, whereas mutant XynA$^{M6\ +\ K99E}$'s half-life was 1.4-fold higher than that of its WT counterpart (Fig. 5 *A*). Interestingly, the mutation K99E in WT xylanase ($t_{1/2} = 30.27$ h) provided thermal stability similar to the thermotolerant M6 xylanase (xylanase WT with six mutations; $t_{1/2} = 33.25$ h). These results indicate that the TKSA-MC approach is a powerful tool for the design of thermal stable enzymes. Moreover, the mutated xylanases were also evaluated in laboratory-scale enzymatic saccharification experiments (Fig. 5 *B*). Using the XynA^{K99E} and XynA$^{M6\ +\ K99E}$ mutants, it was possible to observe an increase in the processivity of DSB near 2.60- and 2.71-fold higher than Celluclast cocktail, respectively. The Celluclast cocktail was able to release a total of 1.76 mg • mL^{-1}, reducing sugars from the DSB at 24 h (Fig. 5 *B*). Besides, XynA^{K99E} and XynA$^{M6\ +\ K99E}$ mutants increase the yield of released sugars by 1.14- and 0.84-fold compared to their nonmutated counterparts, respectively. Thus, K99E appeared to play an essential role in the thermal stability and effective processivity of lignocellulosic biomass. Our data demonstrate that the XynA^{K99E} and XynA$^{M6\ +\ K99E}$ mutants have strong industrial adaptability for use in biofuel and biochemical production from lignocellulosic biomass.

TABLE 3 Kinetic parameters of XynA^{WT}, XynA^{M6}, and mutants

	k_m (mg • mL^{-1})	k_{cat} (s^{-1})
XynA^{WT}	3.34 ± 0.25	485.11 ± 11.37
XynA^{K99E}	3.82 ± 0.14	528.73 ± 6.31
XynA^{M6}	5.89 ± 0.22	239.83 ± 3.46
XynA$^{M6\ +\ K99E}$	8.55 ± 0.33	305.91 ± 5.21

CONCLUSIONS

The computational tractability of the TKSA-MC approach has been shown to be very promising for the protein engineering field. The previous results suggest that surface charge-charge interactions can be redesigned in a rational way to manipulate protein stability (24). Here, the application of TKSA-MC calculation to xylanases identified mutations in the lysine K99 as candidates to increase the enzyme's thermostability. The mutation K99E was performed in the wet lab, and the results showed a nonsignificant increase in the melting temperature ($\Delta Tm \approx 1$). On the other hand, K99E variants present better processability of the DSB and increase the thermotolerance. In other words, the mutated enzymes can keep the catalytic activity for a longer time in comparison with the WT. Notwithstanding that the electrostatics optimization performed by TKSA-MC leads to more stable native state interactions, our observations of the improvement of the catalytic activity are not predictions from the methodology. We hypothesize that the optimized enzyme has a better charge-charge interaction rearrangement, and the new interactions maintain the protein in the functional state for a longer time. Despite the

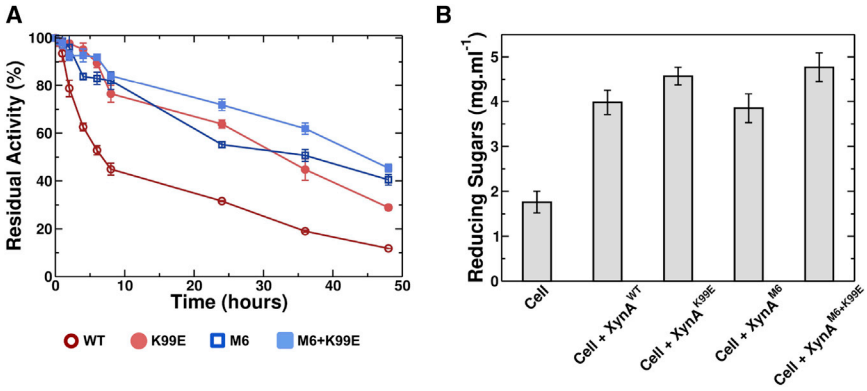

FIGURE 5 Experimental results of the thermal stability assays and saccharification of DSB. (*A*) Residual activity of $XynA^{WT}$, $XynA^{M6}$, and mutants over xylan after incubation at 50°C and pH 5.0 up to 48 h. $XynA^{WT}$, open red circles; e $XynA^{K99E}$, solid red circles; $XynA^{M6}$, open blue squares; $XynA^{M6+K99E}$, solid blue squares. (*B*) Enzymatic hydrolysis reactions in 5.0% (v v^{-1}) of dry biomass and 0.2 FPU g^{-1} of Celluclast enzyme cocktail, supplemented or not with 200 $\mu g \cdot mL^{-1}$ $XynA^{WT}$, $XynA^{M6}$, or mutants, in sodium citrate buffer (50 mM and pH 5.0). The reactions were done in triplicate and incubated at 50°C with agitation during 24 h. To see this figure in color, go online.

small gain in the melting temperature, the achieved results illustrate the applicability of TKSA-MC as an attractive strategy for the design of optimized enzymes for biotechnological purposes. A possible way to improve this approach is to combine it with other bioinformatics methods. One auxiliary candidate could be the usage of the family of homologous proteins to infer consensus and common ancestral sequences, which, along with TKSA-MC results, may provide potential mutations to a specific target protein. Direct-coupling analysis of residue coevolution (48) may also convey information on critical information between correlated mutation residues. Despite the simplicity of the TKSA-MC approach in the way the interactions are considered and the coarse-grained approximations, the method gives remarkably robust results (12,24,40,45). Our results demonstrate the feasibility and applicability of this approach for predicting good mutations based on the pH of the system.

SUPPORTING MATERIAL

Supporting material can be found online at https://doi.org/10.1016/j.bpj.2021.03.036.

AUTHOR CONTRIBUTIONS

V.d.G.C., F.C.R., R.R., and V.B.P.L. designed the research. V.d.G.C., V.M.d.O., and G.G.S. carried out all simulations. F.C.R., R.R.d.M., J.A.S., A.S.d.S., and L.M.Z. performed the experiments. All authors contributed to analyze the data and to write the manuscript.

ACKNOWLEDGMENTS

V.d.G.C. is a Robert A. Welch Postdoctoral Fellow and was also funded by FAPESP (São Paulo Research Foundation Grants 2016/13998-8 and 2017/09662-7 and by CAPES (Coordination for the Improvement of Higher Education Personnel). V.M.d.O. was supported by CNPq (National Council for Scientific and Technological Development) Grant 141985/2013-5 and FAPESP Grant 2018/11614-3. V.B.P.L. was supported by CNPq and FAPESP Grants 2014/06862-7, 2016/19766-1, and 2019/22540-3. R.R.d.M. was supported by FAPESP Grant 2017/14253-9. R.R. was supported by CNPq Grant 429829/2016-7.

REFERENCES

1. Roca, M., H. Liu, …, A. Warshel. 2007. On the relationship between thermal stability and catalytic power of enzymes. *Biochemistry.* 46:15076–15088.
2. Bye, J. W., L. Platts, and R. J. Falconer. 2014. Biopharmaceutical liquid formulation: a review of the science of protein stability and solubility in aqueous environments. *Biotechnol. Lett.* 36:869–875.
3. Huber, K. V., K. M. Olek, …, G. Superti-Furga. 2015. Proteome-wide drug and metabolite interaction mapping by thermal-stability profiling. *Nat. Methods.* 12:1055–1057.
4. Kazlauskas, R. 2018. Engineering more stable proteins. *Chem. Soc. Rev.* 47:9026–9045.
5. Tripathi, S., A. E. Garcìa, and G. I. Makhatadze. 2015. Alterations of nonconserved residues affect protein stability and folding dynamics through charge–charge interactions. *J. Phys. Chem. B.* 119:13103–13112.
6. Wunderlich, M., A. Martin, and F. X. Schmid. 2005. Stabilization of the cold shock protein CspB from Bacillus subtilis by evolutionary optimization of Coulombic interactions. *J. Mol. Biol.* 347:1063–1076.
7. Papaleo, E., M. Olufsen, …, B. O. Brandsdal. 2007. Optimization of electrostatics as a strategy for cold-adaptation: a case study of cold- and warm-active elastases. *J. Mol. Graph. Model.* 26:93–103.
8. Contessoto, V. G., V. M. de Oliveira, …, V. B. Leite. 2016. NTL9 folding at constant pH: the importance of electrostatic interaction and pH dependence. *J. Chem. Theory Comput.* 12:3270–3277.
9. Coronado, M. A., I. P. Caruso, …, R. J. Eberle. 2017. Cold shock protein A from Corynebacterium pseudotuberculosis: role of electrostatic forces in the stability of the secondary structure. *Protein Pept. Lett.* 24:358–367.
10. Bruno da Silva, F., V. G. Contessoto, …, V. B. P. Leite. 2018. Non-native cooperative interactions modulate protein folding rates. *J. Phys. Chem. B.* 122:10817–10824.
11. Lindman, S., W.-F. Xue, …, S. Linse. 2006. Salting the charged surface: pH and salt dependence of protein G B1 stability. *Biophys. J.* 90:2911–2921.
12. Martins de Oliveira, V., V. Godoi Contessoto, …, V. B. Pereira Leite. 2018. Effects of pH and salt concentration on stability of a protein G variant using coarse-grained models. *Biophys. J.* 114:65–75.
13. Yamasaki, M., H. Yano, and K. Aoki. 1990. Differential scanning calorimetric studies on bovine serum albumin: I. Effects of pH and ionic strength. *Int. J. Biol. Macromol.* 12:263–268.

14. Kim, K. S., S. Kim, …, D. Y. Kwon. 2004. Changes of glycinin conformation due to pH, heat and salt determined by differential scanning calorimetry and circular dichroism. *Int. J. Food Sci. Technol.* 39:385–393.

15. Bye, J. W., and R. J. Falconer. 2013. Thermal stability of lysozyme as a function of ion concentration: a reappraisal of the relationship between the Hofmeister series and protein stability. *Protein Sci.* 22:1563–1570.

16. Dumorné, K., D. C. Córdova, …, P. Renganathan. 2017. Extremozymes: a potential source for industrial applications. *J. Microbiol. Biotechnol.* 27:649–659.

17. Ruller, R., L. Deliberto, …, R. J. Ward. 2008. Thermostable variants of the recombinant xylanase A from Bacillus subtilis produced by directed evolution show reduced heat capacity changes. *Proteins.* 70:1280–1293.

18. Ruller, R., J. Alponti, …, R. J. Ward. 2014. Concommitant adaptation of a GH11 xylanase by directed evolution to create an alkali-tolerant/thermophilic enzyme. *Protein Eng. Des. Sel.* 27:255–262.

19. Cherry, J. R., and A. L. Fidantsef. 2003. Directed evolution of industrial enzymes: an update. *Curr. Opin. Biotechnol.* 14:438–443.

20. Porter, J. L., R. A. Rusli, and D. L. Ollis. 2016. Directed evolution of enzymes for industrial biocatalysis. *ChemBioChem.* 17:197–203.

21. Jemli, S., D. Ayadi-Zouari, …, S. Bejar. 2016. Biocatalysts: application and engineering for industrial purposes. *Crit. Rev. Biotechnol.* 36:246–258.

22. Marabotti, A., B. Scafuri, and A. Facchiano. 2020. Predicting the stability of mutant proteins by computational approaches: an overview. *Brief. Bioinform* bbaa074, Published online June 3, 2020.

23. da Silva, F. B., V. M. de Oliveira, …, V. B. P. Leite. 2020. Rational design of chymotrypsin inhibitor 2 by optimizing non-native interactions. *J. Chem. Inf. Model.* 60:982–988.

24. Gribenko, A. V., M. M. Patel, …, G. I. Makhatadze. 2009. Rational stabilization of enzymes by computational redesign of surface charge-charge interactions. *Proc. Natl. Acad. Sci. USA.* 106:2601–2606.

25. Makhatadze, G. I. 2017. Linking computation and experiments to study the role of charge-charge interactions in protein folding and stability. *Phys. Biol.* 14:013002.

26. Permyakov, S. E., G. I. Makhatadze, …, L. J. Berliner. 2005. How to improve nature: study of the electrostatic properties of the surface of α-lactalbumin. *Protein Eng. Des. Sel.* 18:425–433.

27. Kirkwood, J. G. 1934. Theory of solutions of molecules containing widely separated charges with special application to zwitterions. *J. Chem. Phys.* 2:351–361.

28. Tanford, C., and J. G. Kirkwood. 1957. Theory of protein titration curves. I. General equations for impenetrable spheres. *J. Am. Chem. Soc.* 79:5333–5339.

29. Shire, S. J., G. I. Hanania, and F. R. Gurd. 1974. Electrostatic effects in myoglobin. Hydrogen ion equilibria in sperm whale ferrimyoglobin. *Biochemistry.* 13:2967–2974.

30. Havranek, J. J., and P. B. Harbury. 1999. Tanford-Kirkwood electrostatics for protein modeling. *Proc. Natl. Acad. Sci. USA.* 96:11145–11150.

31. Contessoto, V. G., V. M. de Oliveira, …, V. B. P. Leite. 2018. TKSA-MC: a web server for rational mutation through the optimization of protein charge interactions. *Proteins.* 86:1184–1188.

32. Malgas, S., M. S. Mafa, …, B. I. Pletschke. 2019. A mini review of xylanolytic enzymes with regards to their synergistic interactions during hetero-xylan degradation. *World J. Microbiol. Biotechnol.* 35:187.

33. Pettersen, E. F., T. D. Goddard, …, T. E. Ferrin. 2004. UCSF Chimera–a visualization system for exploratory research and analysis. *J. Comput. Chem.* 25:1605–1612.

34. Murakami, M. T., R. K. Arni, …, R. J. Ward. 2005. Correlation of temperature induced conformation change with optimum catalytic activity in the recombinant G/11 xylanase A from Bacillus subtilis strain 168 (1A1). *FEBS Lett.* 579:6505–6510.

35. Silva, S. B., M. P. Pinheiro, …, R. J. Ward. 2017. The role of local residue environmental changes in thermostable mutants of the GH11 xylanase from Bacillus subtilis. *Int. J. Biol. Macromol.* 97:574–584.

36. Webb, B., and A. Sali. 2016. Comparative protein structure modeling using MODELLER. *Curr. Protoc. Bioinformatics.* 54:5.6.1–5.6.37.

37. Orttung, W. H. 1970. Proton binding and dipole moment of hemoglobin. Refined calculations. *Biochemistry.* 9:2394–2402.

38. Tanford, C., and R. Roxby. 1972. Interpretation of protein titration curves. Application to lysozyme. *Biochemistry.* 11:2192–2198.

39. Bashford, D., and M. Karplus. 1991. Multiple-site titration curves of proteins: an analysis of exact and approximate methods for their calculation. *J. Phys. Chem.* 95:9556–9561.

40. Ibarra-Molero, B., V. V. Loladze, …, J. M. Sanchez-Ruiz. 1999. Thermal versus guanidine-induced unfolding of ubiquitin. An analysis in terms of the contributions from charge-charge interactions to protein stability. *Biochemistry.* 38:8138–8149.

41. Strickler, S. S., A. V. Gribenko, …, G. I. Makhatadze. 2006. Protein stability and surface electrostatics: a charged relationship. *Biochemistry.* 45:2761–2766.

42. Herlet, J., P. Kornberger, …, V. V. Zverlov. 2017. A new method to evaluate temperature vs. pH activity profiles for biotechnological relevant enzymes. *Biotechnol. Biofuels.* 10:234.

43. Miller, G. L. 1959. Use of dinitrosalicylic acid reagent for determination of reducing sugar. *Anal. Chem.* 31:426–428.

44. Nguyen, C., J. T. Young, …, M. E. McCully. 2019. A dynamic hydrophobic core and surface salt bridges thermostabilize a designed three-helix bundle. *Biophys. J.* 116:621–632.

45. Ibarra-Molero, B., and J. M. Sanchez-Ruiz. 2002. Genetic algorithm to design stabilizing surface-charge distributions in proteins. *J. Phys. Chem. B.* 106:6609–6613.

46. Makhatadze, G. I., V. V. Loladze, …, S. T. Thomas. 2003. Contribution of surface salt bridges to protein stability: guidelines for protein engineering. *J. Mol. Biol.* 327:1135–1148.

47. Ruller, R., J. C. Rosa, …, R. J. Ward. 2006. Efficient constitutive expression of Bacillus subtilis xylanase A in *Escherichia coli* DH5α under the control of the Bacillus BsXA promoter. *Biotechnol. Appl. Biochem.* 43:9–15.

48. Morcos, F., A. Pagnani, …, M. Weigt. 2011. Direct-coupling analysis of residue coevolution captures native contacts across many protein families. *Proc. Natl. Acad. Sci. USA.* 108:E1293–E1301.